ЖЭТФ, 2014, том 145, вып. 5, стр. 838–850

FRACTALS OF GRAPHENE QUANTUM DOTS IN PHOTOLUMINESCENCE OF SHUNGITE

B. S. Razbirin [a], ***N. N. Rozhkova*** [b], ***E. F. Sheka*** [c*], ***D. K. Nelson*** [a], ***A. N. Starukhin*** [a]

[a] *Ioffe Physical-Technical Institute, Russian Academy of Sciences*
194021, Saint Petersburg, Russia

[b] *Institute of Geology, Karelian Research Centre, Russian Academy of Sciences*
185910, Petrozavodsk, Russia

[c] *Peoples' Friendship University of Russia*
117198, Moscow, Russia

Received August 12, 2013

Viewing shungite as loosely packed fractal nets of graphene-based (reduced graphene oxide, rGO) quantum dots (GQDs), we consider photoluminescence of the latter as a convincing proof of the structural concept as well as of the GQD attribution to individual rGO fragments. We study emission from shungite GQDs for colloidal dispersions in water, carbon tetrachloride, and toluene at both room and low temperatures. As expected, the photoluminescence of the GQD aqueous dispersions is quite similar to that of synthetic GQDs of the rGO origin. The morphological study of shungite dispersions shows a steady trend of GQDs to form fractals and to drastically change the colloid fractal structure caused by the solvent exchange. Spectral study reveals a dual character of the emitting centers: individual GQDs are responsible for the spectra position while the fractal structure of GQD colloids provides high broadening of the spectra due to structural inhomogeneity, thus causing a peculiar dependence of the photoluminescence spectra on the excitation wavelength. For the first time, photoluminescence spectra of individual GQDs were observed in frozen toluene dispersions, which paves the way for a theoretical treatment of the GQD photonics.

DOI: 10.7868/S0044451014050073

1. INTRODUCTION

Originally, the term "graphene quantum dot" (GQD) appeared in theoretical research and was attributed to fragments limited in size, or domains, of a single-layer two-dimensional graphene crystal. The subject of the investigations concerned the quantum size effects, manifested in the spin [1, 2], electronic [3] and optical [4–9] properties of the fragments. These studies significantly stimulated the interest in GQDs and their attractive applications (see, e. g., [10] and the references therein), which raised the question of their preparation. This proved to be a difficult task and the progress achieved by now has been presented in exhaustive reviews [11, 12]. On the basis of spectral studies, we have found that in almost all cases, the GQDs are not single-layer graphene domains but multi-layer formations containing up to 10 layers of reduced graphene oxide (rGO) of less than 30 nm in size.

Optical spectroscopy, and photoluminescence (PL) in particular, was the primary method of studying the properties of the GQDs. Review [12] presents a complete picture of the results, which can be summarized as follows.

1. Regardless of the method of obtaining GQDs in water solution, the final product is a mixture of particles differing in size (both width and thickness).

2. Morphology of GQDs reveals that the particle size is not determined by the production process, although depending on the starting materials. The average linear dimension is about 10 nm, while the maximum is 60 nm. The average thickness of particles indicates multi-layer, in most cases, five-layer GQDs, although obtaining single-layer GQDs is also not uncommon (see, e. g. [13–17]).

3. Fourier-transform infrared spectroscopy and

*E-mail: sheka@icp.ac.ru

photoelectron spectra show that in almost all the cases studied, the chemical composition of GQDs corresponds to partially oxidized graphene.

4. The absorption spectra in the visible and UV range show a well-marked size effect that is manifested as a red shift of the spectrum with increasing the GQD size.

A detailed description of these features with the presentation of their possible explanations and links to the relevant publications is given in [12].

As seen from the synopsis, optical spectroscopy of GQDs gives a complicated picture with many features. However, in spite of this diversity, common patterns can be identified that can be the basis of the GQD spectral analysis. These general characteristics include: (1) structural inhomogeneity of GQD solutions, which should rather be called dispersions; (2) low-concentration limit that provides surveillance of the PL spectra; (3) dependence of the GQD PL spectrum on the solvent, and (4) dependence of the GQD PL spectrum on the excitation light wavelength. It is these four circumstances that determine usual conditions under which the spectral analysis of complex polyatomic molecules is performed. The condition optimization, primarily including the choice of solvent and the experiment performance at low temperature, in many cases led to good results, based on structural PL spectra (see, e. g., the relevant research of fullerene solutions [18–21]). In this paper, we show that implementing this optimization for the spectral analysis of GQDs turns out to be quite successful.

2. GRAPHENE QUANTUM DOTS OF NATURAL ORIGIN

Synthetic GQDs described in the preceding section have recently been complemented with GQDs of natural origin [22, 23]. It has been shown that GQDs present the main structural peculiarity of shungite of Karelian deposits. Based on the detailed analysis of physical and chemical properties of graphene and its derivations, it was established in [22] that shungite should be regarded as one of the natural carbon allotropes, possessing multistage fractal nets of rGO fragments less than 1 nm in size. The generality of the basic structural elements of shungite and synthetic GQDs as well as the ability of the former to disperse in water provided a basis of a research project [23] aimed at establishing the generality of the spectral properties of aqueous dispersions of shungite and synthetic GQDs and proving the structural formula of shungite given above. The conducted spectral studies provided the desired confirmation, at the same time exhibiting particular features of the observed spectral characteristics that allowed insights into the structural and spectral peculiarities of the GQDs dissolved in different solvents.

3. FRACTAL NATURE OF THE OBJECT UNDER STUDY

The GQD concept evidently implies a dispersed state of a number of nanosize rGO fragments. Empirically, the state is provided by the fragment dissolution in a solvent. Once dissolved, the fragments unavoidably aggregate, forming colloidal dispersions. As mentioned above, so far only aqueous dispersions of synthetic GQDs have been studied [11, 12]. In the case of shungite GQDs, two molecular solvents, carbon tetrachloride and toluene, were used to replace water in the pristine dispersions. In each of these cases, the colloidal aggregates are the main object of study. Although there has been no direct confirmation of their fractal structure, there are serious reasons to suppose that it is an obvious reality. Actually, first, the fragment formation occurred under conditions that unavoidably involve elements of randomness in the course of both laboratory chemical reactions and natural graphitization [22]; the latter concerns the fragment size and shape. Second, the fragment structure certainly bears the stamp of polymers, for which fractal structure of aggregates in dilute dispersions has been convincingly proved (see [24] and the references therein).

As shown in [24], the fractal structure of colloidal aggregates is highly sensitive to the ambient solvent, the temperature of the aggregates formation, and other external actions such as mechanical stress and so forth. This fact makes the definition of quantum dots of colloidal dispersions rather vague at the structural level. In the case of GQDs of different origin, the situation is additionally complicated because the aggregation of synthetic (Sy) and shungite (Sh) rGO fragments occurred under different external conditions. In view of this, it must be assumed that rGO-Sy and rGO-Sh aggregates of not only different but also the same solvent dispersions are quite different.

Seeking the answer to the question of whether the same term GQD can be attributed to colloidal dispersion in the above two cases, we should recall that a feature of fractal structures is that fractals are typically self-similar patterns, where "self-similar" means that they are "the same from near as from far" [25]. This means that the peculiarities, e. g., of the optical

behavior of each of the two rGO-Sy and rGO-Sh colloidal dispersions obey the same law. From this standpoint, there apparently is no difference which structural element of a multilevel fractal structure of their colloidal aggregates should be attributed to a quantum dot. However, the identity of both final and intermediate fractal structures of aggregates in different solvents is highly questionable and only the basic rGO structural units can be identified without a doubt. Therefore, GQDs of both rGO-Sy and rGO-Sh dispersions should associate with rGO individual fragments. This is why different fractal nets of GQDs provided by different colloidal dispersions are the object of this study. As regards the spectral behavior of the dispersions, we should expect an obvious generality provided by the common nature of GQDs, but simultaneously complicated by the difference in fractal packing of the dots in the different-solvent dispersions. The latter mainly concerns the rGO-Sh dispersions [23] that are considered in detail below.

4. rGO-Sh AQUEOUS DISPERSIONS

In full agreement with commonly used methods for the preparation of colloidal dispersions of graphene and its derivatives [26, 27], rGO-Sh aqueous dispersions were obtained by sonication of the pristine shungite powder for 15 min with an ultrasonic disperser UZ-2M (at a frequency 22 kHz and the operating power 300 W) followed by filtration and ultracentrifugation [28]. The maximum achievable concentration of carbon is less than 0.1 mg/ml, which is consistent with poor water solubility of graphene and its derivatives [26]. The resulting dispersions are quite stable, and their properties vary little during the time. The size-distribution characteristic profile of rGO-Sh aggregates is shown in Fig. 1*a*. It was obtained by dynamic light scattering using nanoparticle size analyzer Zetasizer Nano ZS (Malvern Instruments). The results were processed in the approximation of a spherical shape of the aggregates. As can be seen from the figure, the average size of the aggregates is 54 nm, whereas the distribution is quite broad, 26 nm, such that the resulting colloids are significantly inhomogeneous. The inhomogeneity obviously concerns both size and shape of basic rGO fragments and, consequently, GQDs. The structure of the carbon condensate formed after water evaporation from the dispersion droplets on a glass substrate is shown in Figs. 1*b* and 1*c*. As can be seen from the figure, the condensate has a fractal structure formed by aggregates, whose shape is close to spherical. It should be mentioned that the condensate fractal structure should not be identical to that of the pristine dispersion [24], although, no doubt, some continuity of the structure should be manifested.

Figure 2*a* shows an overview on the characteristic patterns of the emission spectrum of rGO-Sh aqueous dispersions at different excitation wavelength λ_{exc} at 80 K. Increasing the temperature to 293 K does not cause a significant change in the spectra, resulting in only a slight broadening of their structural component related to the Raman spectrum of water at the fundamental frequency $\sim$ 3400 cm^{-1} of the O–H stretching vibrations. When excited at λ_{exc} = 405 and λ_{exc} = 457 nm, the Raman spectrum superimposes a broad luminescence band in the range 17000–22000 cm^{-1}. The emission of the dispersion at λ_{exc} = 532 nm is weak. Figure 2*b* shows the PL spectra of the aqueous dispersion at λ_{exc} = 405 and λ_{exc} = 457 nm after subtracting the Raman spectrum of water. Both spectra are broad and bell-shaped that is characteristic of the PL spectra of rGO-Sy aqueous dispersions (see [12]). In spite of the large width of PL spectra, their position in the same spectral region for both rGO-Sy and rGO-Sh aqueous dispersions evidences a common nature of the emitting GQDs.

The similarity of the spectral behavior of the two dispersions also extends to a considerable overlap of their absorption and PL spectra, so that a set of new PL spectra can be excited with an increase in λ_{exc} within practically each PL spectrum. Of course, a shift of these new PL spectra maxima toward longer wavelengths with increasing λ_{exc} is observed. Such a behavior usually indicates the presence of an inhomogeneously broadened absorption spectrum of the emitters that widely overlaps with the PL one and whose excitation at different λ_{exc} within the overlapping region results in the selective excitation of different sets of emitting centers. In the case of rGO-Sy dispersions, the spectrum inhomogeneous broadening is usually explained by scatter in the GQDs (rGO fragments) linear dimensions [12]. However, not only GQDs linear dimensions but also their shape and the composition of colloidal aggregates may largely vary, which should be expected for the rGO-Sh dispersions, in particular. This is clearly seen in the example of various aggregate structures of the condensates shown above in Figs. 1*b* and 1*c*. Unfortunately, the large width of PL spectra does not allow exhibiting those spectral details that might speak about the aggregated structure of GQDs.

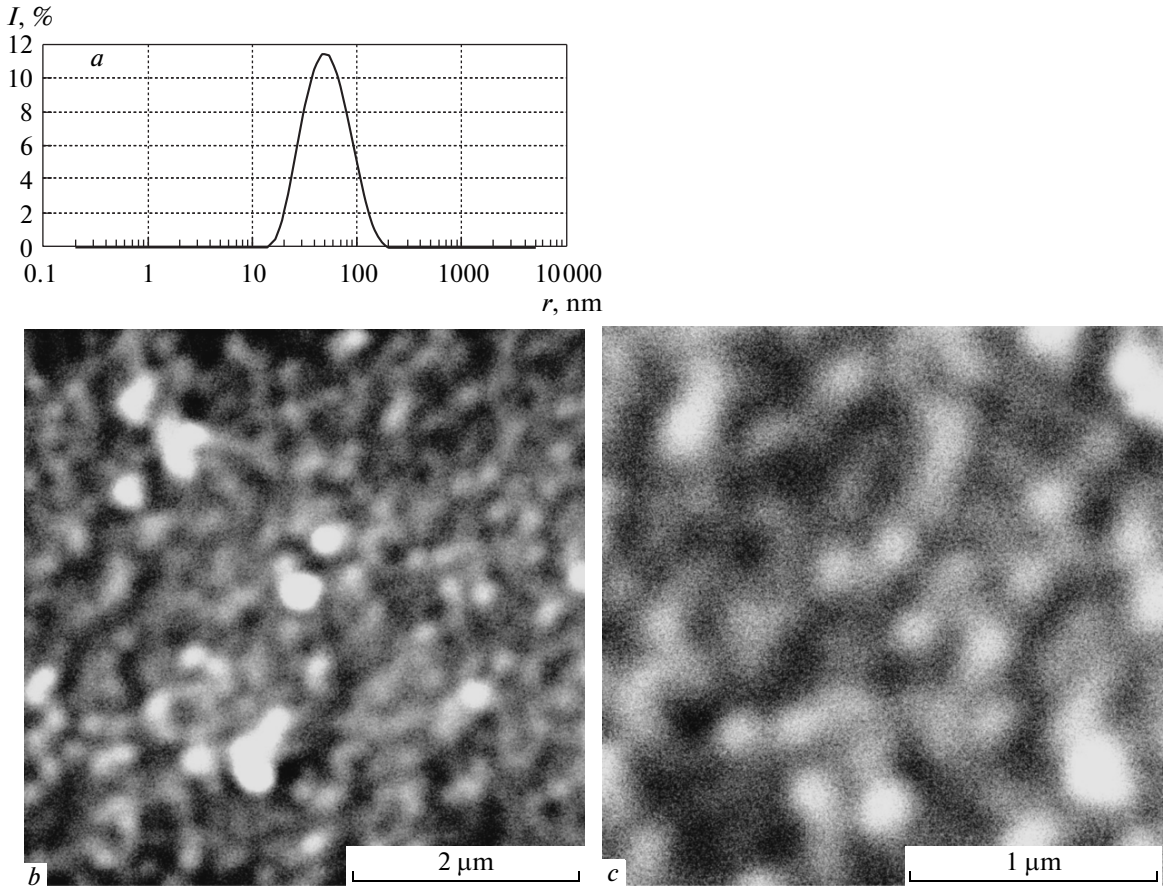

Fig. 1. (a) Size-distribution profile of colloidal aggregates in shungite aqueous dispersion, (b and c) scanning electron microscope (SEM) images of the dispersion condensate on a glass substrate in different scales. Carbon concentration is 0.1 mg/ml

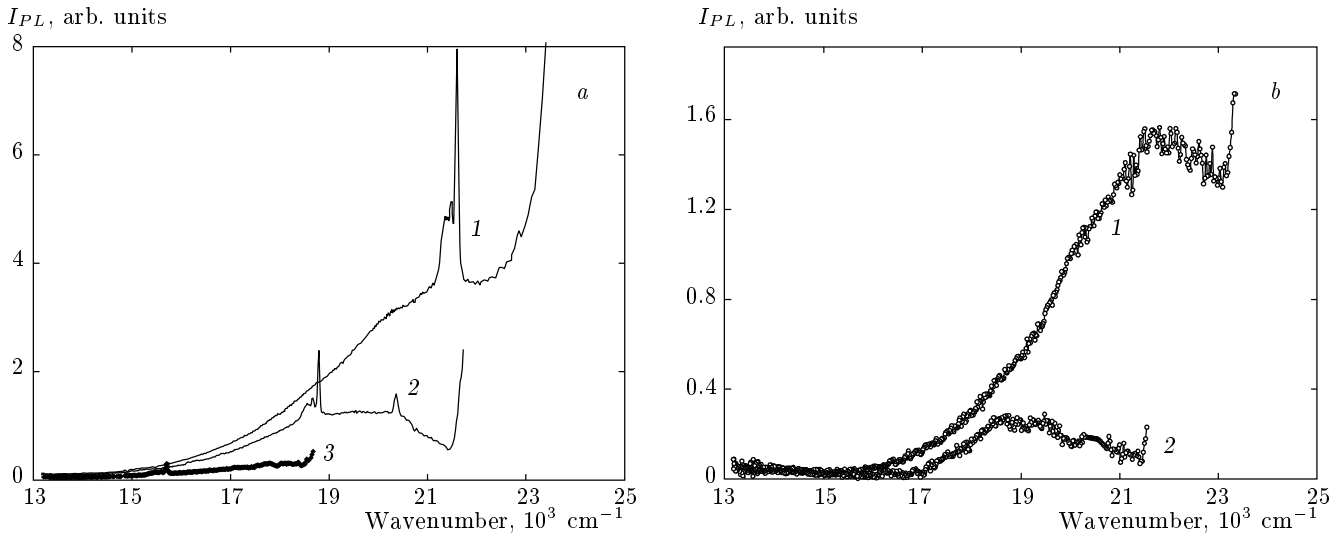

Fig. 2. Photoluminescence spectra of shungite aqueous dispersions at 80 K (a) as observed and (b) after subtraction of Raman scattering of water. Excitation wavelengths (*1*) 405 nm; (*2*) 457 nm; (*3*) 532 nm

5. rGO-Sh DISPERSIONS IN ORGANIC SOLVENTS

Traditionally, the best way to overcome difficulties caused by inhomogeneous broadening of optical spectra of complex molecules is the use of their dispersions in frozen crystalline matrices. The choice of solvent is highly important. For example, water is a "bad" solvent because the absorption and emission spectra of dissolved large organic molecules are usually broadband and unstructured. By contrast, frozen solutions of complex organic molecules, e. g., including fullerenes [18–21], in carbon tetrachloride (CTC) or toluene (T), in some cases provide a reliable monitoring of fine-structured spectra of individual molecules (Shpolskii's effect [29]). Detection of PL structural spectra or structural components of broad PL spectra not only simplifies spectral analysis but also indicates the dispersing of emitting centers into individual molecules. It is this fact that was the basis of the solvent choice in studying spectral properties of shungite GQDs [23].

Organic rGO-Sh dispersions were prepared from the pristine aqueous dispersions in the course of sequential replacement of water first by isopropyl alcohol and then by CTC or T [30]. The morphology and spectral properties of these dispersions turned out to be different, and we therefore discuss them separately.

5.1. rGO-Sh dispersions in carbon tetrachloride

When analyzing CTC-dispersion morphology, a drastic change in the size-distribution profiles of the dispersion aggregates compared with that of aqueous dispersions (Fig. 3) was the first highly important result. The second result concerns the high incertitude in this fractal structure. Figures 3*a* and 3*b* present size-distribution profiles related to CTC-dispersions most different with rspect to this parameter. Figures 3*c* and 3*d* show images of agglomerates of films obtained when drying the CTC-dispersion droplets on glass. As can be seen by comparing Fig. 1 and Fig. 3, the average colloidal aggregate size increases when water is substituted by CTC. The nearly spherical shape of aggregates in Figs. 1*b* and 1*c* is replaced by lamellar faceting, mostly characteristic of microcrystals. Noteworthy is the absence of small aggregates, which indicates a complete absence of individual GQDs in the dispersions. Therefore, the change in size-distribution profiles as well as in the shape of the aggregates of the condensate evidences a strong influence of solvent on the aggregate structure, thus decisively confirming that the interaction between GQDs is stronger than between GQDs and solvent molecules.

The conducted spectral studies are quite consistent with these findings. The dispersions have a faint yellow-brown color, which indicates the presence of significant absorption of the solutions in the visible range (Fig. 4*a*). The PL spectra were studied for a wide range of dispersions obtained at different time. As found, both the behavior of these spectra at different exciting-laser wavelengths λ_{exc} and the shape of PL spectra of different dispersions are largely similar, while the spectra intensity can differ substantially. Arrows in Fig. 4*a* show the wavenumber values λ_{exc}^{-1} corresponding to laser lines at λ_{exc} = 405, 457, 476.5, 496.5, 514.5, 532 nm.

Figure 4 shows PL spectra of CTC-dispersion DC1, whose morphological properties are close to those shown in Fig. 3*a*. As we see from Fig. 4*a*, the dispersion absorption increases when advancing to the UV region. It can be assumed that the absorption of each component of the aggregate conglomerate increases with decreasing λ_{exc}, and therefore the excitation with UV light at λ_{exc} = 337.1 nm affects almost all the emitting centers in the crystal matrix. Actually, the UV-excited PL spectrum in Fig. 4*a* is very broad and covers the region from 27000 to 15000 cm^{-1}. In this case, the PL spectrum overlaps with the absorption spectrum over the entire spectral range. Such a large overlap evidences the inhomogeneously broadened character of both spectra, that is, the formation of an ensemble of emitting centers that differ in the probability of emission (absorption) at a given wavelength (it is assumed that the probability of energy migration between the centers is low). Indeed, successive PL excitation by laser lines *1*, *3*, *4*, and *5* (see Fig. 4*a*) causes a significant modification of the PL spectra (Fig. 4*b*). The width of the spectra decreases as λ_{exc} increases, the PL band maximum is shifted to longer wavelengths, and the spectrum intensity decreases. This is due to selective excitation of a certain group of centers. In general, the observed pattern is typical for structurally disordered systems discussed in the preceding section. To simplify the subsequent comparative analysis of the spectra obtained at different λ_{exc}, we let them be denoted in accordance with the excitation wavelength: 405-, 476-, 496-spectrum, etc.

Comparing the PL spectra of dispersion DC1 at different excitations, we note that (1) PL spectra obtained when excited in the overlap region of the absorption and emission spectra in Fig. 4*a*, have a more distinct structure than the 337-spectrum, but still evidence a superpositioning character of the spectra; (2) the intensity of the 405-spectrum is almost an order of magnitude higher than the intensity of the rest of the spectra.

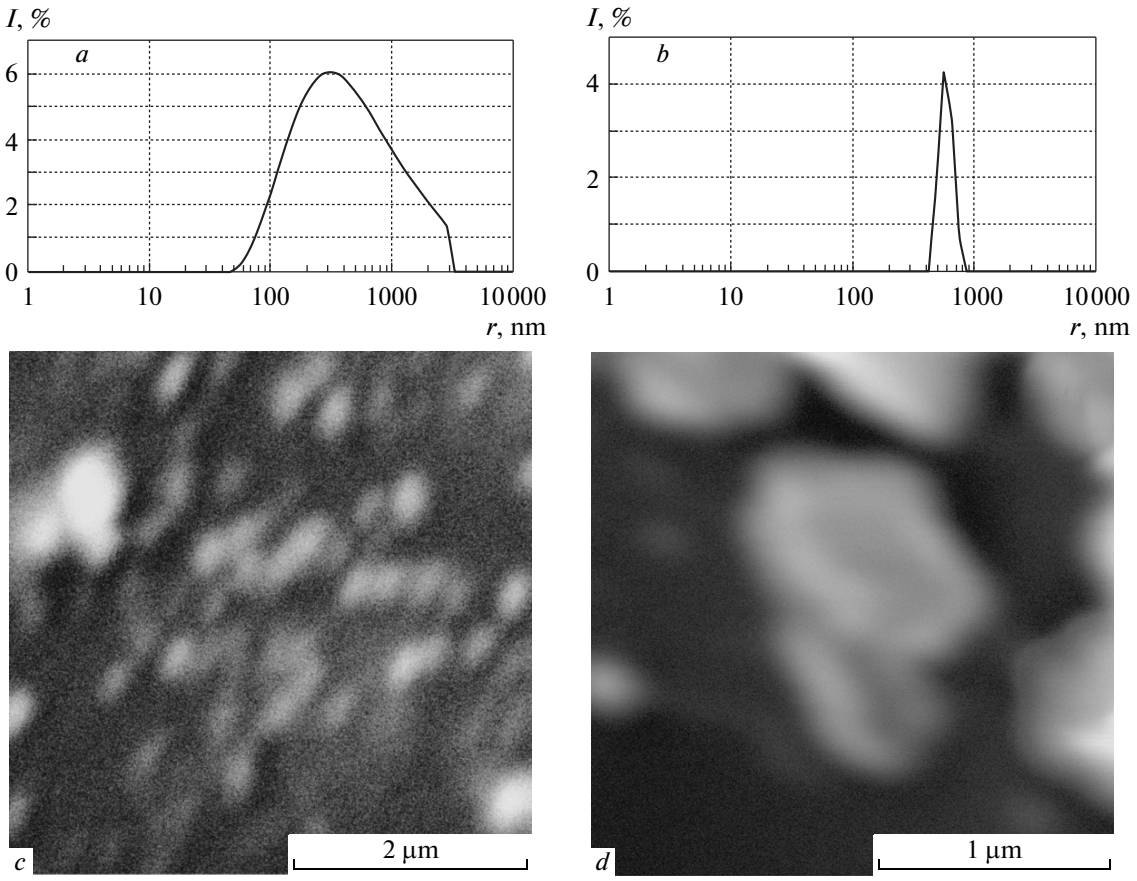

Fig. 3. (a and b) Size-distribution profiles of colloidal aggregates in shungite dispersion in carbon tetrachloride; (c and d) SEM images of the dispersion condensates on glass substrate in different scales

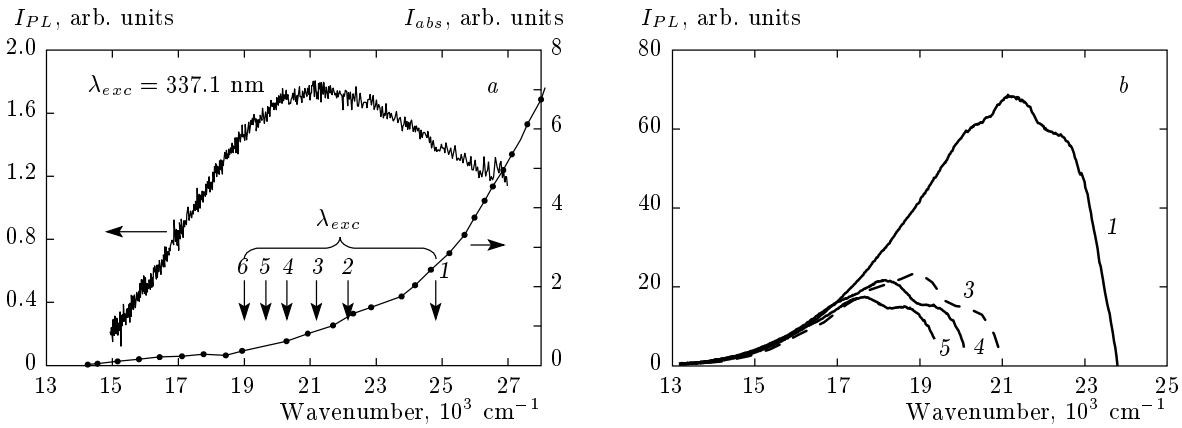

Fig. 4. (a and b) Photoluminescence and (a) absorption spectra of shungite dispersion in carbon tetrachloride DC1 at 80 K after the background emission subtraction. Numbers from *1* to *6* mark excitation wavelengths (*1*) $\lambda_{exc} = 405.0$ nm, (*2*) 457.0 nm, (*3*) 476.5 nm, (*4*) 496.5 nm, (*5*) 514.5 nm, (*6*) 532.0 nm

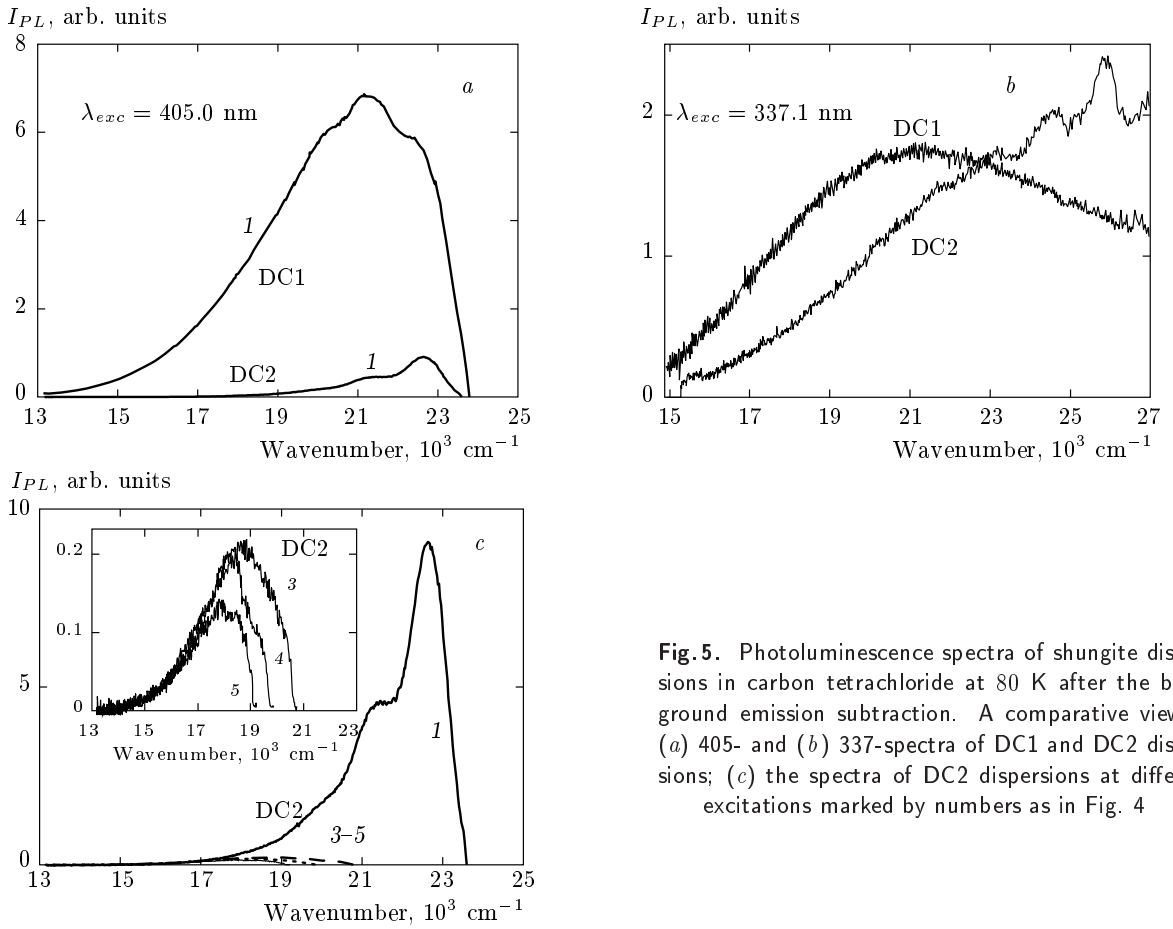

Fig. 5. Photoluminescence spectra of shungite dispersions in carbon tetrachloride at 80 K after the background emission subtraction. A comparative view of (*a*) 405- and (*b*) 337-spectra of DC1 and DC2 dispersions; (*c*) the spectra of DC2 dispersions at different excitations marked by numbers as in Fig. 4

Before discussing the features of the observed spectra, we consider the PL spectra of dispersion DC2 that is close in morphology to the dispersion shown in Fig. 3*b*. Figures 5*a* and 5*b* compare the 405- and 337-spectra of DC2 with those of DC1 described above. The 337-spectrum of DC2 exhibits a new UV band, the intensity of its 405-spectrum decreases by several times. However, it is important to note that the 405-spectrum of DC2 is still the most intense among other spectra (Fig. 5*c*). The spectrum of DC2 still retains a three-peak shape, but their intensities are significantly redistributed. Apparently, the difference between DC1 and DC2 spectra speaks about a redistribution of the GQD sets in the two dispersions.

Comparative analysis of the PL spectra of dispersions DC1 and DC2 shows that the above- mentioned spectral regularities are sensitive to the structure of CTC dispersions and are directly related to the degree of structural inhomogeneity. Thus, narrowing the size-distribution profile related to dispersion DC2 undoubtedly causes the narrowing of inhomogeneously broadened absorption and emission spectra, such that the intensity of the long-wavelength emission spectra of DC2 dispersion decreases. Because of the cutoff of the long-wavelength absorption spectrum of DC2 dispersion, the structure of its 405-spectrum becomes more noticeable, apparently due to an additional feature of the distribution of emitting centers in DC2 over energy. Unchanged in both sets of spectra is the predominance intensity of the 405-spectrum.

The difference in the structural inhomogeneity of dispersions raises the question of their temporal stability. Spectral analysis of their PL allows answering this question. In Fig. 6, we return to dispersion DC1, but after 1.5 years (dispersion DC1*). As can be seen from Fig. 6*a*, the PL spectrum of DC1* reveals the appearance of new emitting centers, responsible for PL in the UV region. The rest of the 337-spectrum does not change much, preserving its intensity and large width. Changes in PL spectra in the visible range are less pronounced (Fig. 6*b*). Attention is drawn to the high intensity of the 457-spectrum of DC1*.

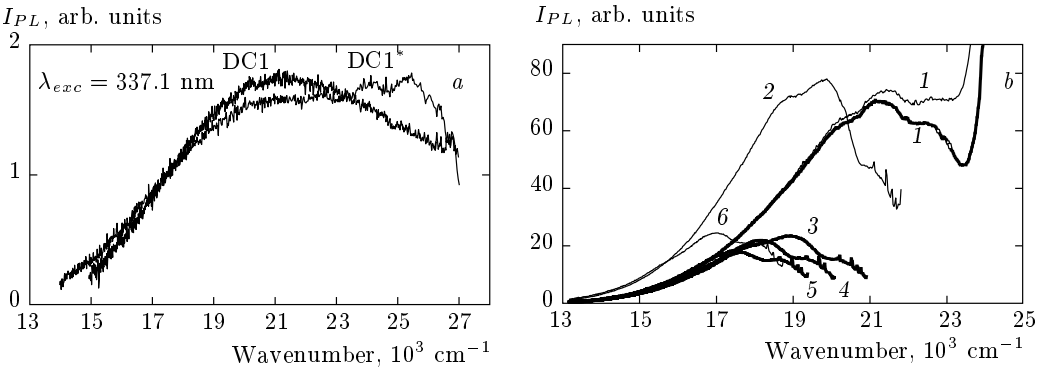

Fig. 6. Photoluminescence spectra of shungite dispersions in carbon tetrachloride at 80 K after the background emission subtraction. (a) A comparative view of 337-spectra of DC1 and DC1* dispersions; (b) the same for spectra of DC1 (thick curves) and DC1* (thin curves) dispersions at different excitations marked by numbers as in Fig. 4

Thus, the set of PL spectra obtained for rGO-Sh CTC-dispersions allows making the following conclusions.

1. None of fine-structured spectra similar to Shpolskii's spectra of organic molecules was observed in the low-temperature PL spectra of crystalline CTC-dispersions. This is consistent with the absence of small particles in the size-distribution profiles of the relevant colloidal aggregates.

2. The PL spectra are broad and overlap with the absorption spectrum over a wide spectral range. This fact testifies to the inhomogeneous broadening of the spectra, which is the result of a nonuniform distribution of the dispersion colloidal aggregates, confirmed by morphological measurements.

3. The observed high sensitivity of PL spectra to the structural inhomogeneity of dispersions allows using the fluorescent spectral analysis as a method for tracking the process of the formation of primary dispersions and their aging over time.

4. Selective excitation of emission spectra by different laser lines allows decomposing the total spectrum into components corresponding to the excitation of different groups of emitting centers. In this case, common to all the studied dispersions is the high intensity of the emission spectra excited at $\lambda_{exc} = 405$ and $\lambda_{exc} = 457$ nm.

5.2. rGO-Sh dispersion in toluene

The behavior of toluene rGO-Sh dispersions is more intricate from both morphological and spectral standpoints. Basic GQDs of aqueous dispersions are nearly insoluble in toluene, and therefore the resulting toluene dispersions are essentially colorless due to the low concentration of the solute. In addition, the low concentration makes the dispersion very sensitive to any change in both the content and structure. This causes structural instability of dispersions, which is manifested, in particular, in the time dependence of the relevant size-distribution profiles. Thus, the three-peak distribution of the initial toluene dispersion shown in Fig. 7a is gradually replaced by a single-peaked distribution in Fig. 7b in one to two hours. The last distribution does not change with time and represents the distribution of the solute in the supernatant.

Similarly to carbon tetrachloride, toluene causes a drastic change in the colloidal aggregates structure thus once again proving the fractal structure of the pristine GQD colloids in aqueous dispersions. However, if the carbon tetrachloride action can be attributed to the consolidation of the pristine colloids, the toluene results in a quite opposite effect, leading to their dispersing, which indicates that the interaction between GQDs is weaker than between GQDs and toluene molecules. The three-peak structure in Fig. 7a shows that at the initial stage of water replacement by toluene, in the resulting liquid medium, there are three kinds of particles with average linear dimensions of about 2.5, 70, and 1100 nm. All the three sets are characterized by a wide scatter. Large particles are seen in the electron microscope (Figs. 7c and 7d) as freaky sprawled fragments. Over time, these three entities are replaced by one with an average size of about 0.25 nm. Thus, freshly produced dispersions containing GQD aggregates of varying complexity turns into the dispersion of individual GQDs. We note that the obtained average size seems to be too small. This might be because the program processing of the particle distribution in Zetasizer Nano ZS (Malvern Instruments) is based on

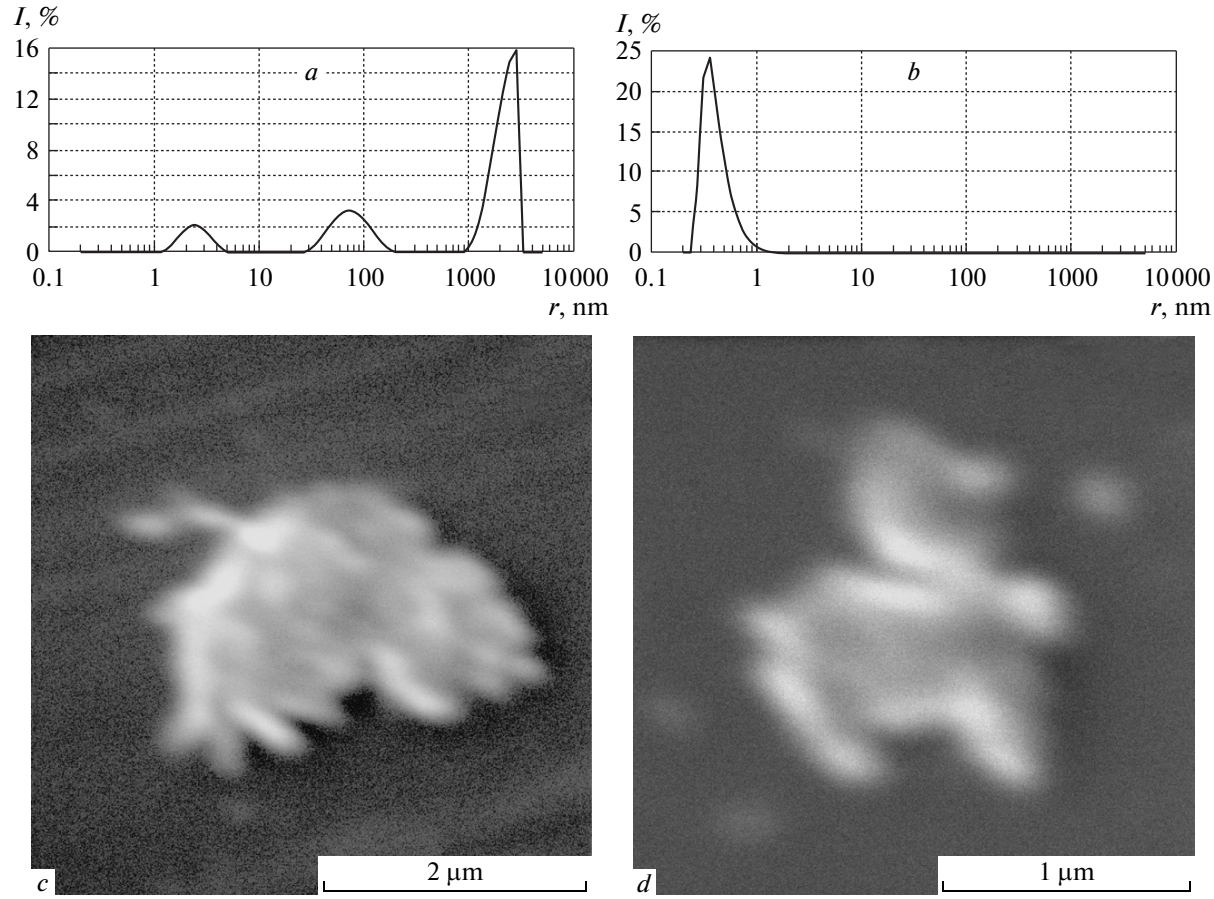

Fig. 7. (a and b) Size-distribution profiles of colloidal aggregates in shungite toluene dispersion; (c and d) SEM images of the dispersion condensates on glass substrate in different scales. Carbon concentrations are (a) 0.08 mg/ml and (b) 0.04 mg/ml

the approximation of spherical three-dimensional particles, whereby the output data can be assigned to the two-dimensional structural anisotropic particles with a big stretch. Hence the value 0.25 nm can be accepted as a very approximate one and only consistent by the order of magnitude with the empirical value of about 1 nm for the average size of GQDs in shungite [22].

The conversion of the aqueous dispersion of aggregated GQDs into the colloidal dispersion of individual GQDs in toluene is a peculiar manifestation of the interaction of solvents with fractals described in [24]. Apparently, GQD fractals are differently "opaque" or "transparent" with respect to carbon tetrachloride and toluene, which causes such a big effect. Certainly, this finding may stimulate the consideration of nanosize graphene dispersions in the framework of fractal science similarly to the polymer study [24]. As regards graphene photonics, the obtained toluene dispersion has allowed investigating individual GQDs for the first time.

Figure 8 shows the PL spectra of colloidal dispersions of individual GQDs in toluene. The *brutto* experimental spectra, each of which is a superposition of the Raman spectrum of toluene and the PL spectrum of the dispersion, are presented in Fig. 8a. We note the clearly visible enhancement of Raman scattering of toluene in the range 20000–17000 cm^{-1}. Figure 8b shows the PL spectra after subtracting the Raman spectra. The spectra presented in the figure can be divided into three groups. The first group includes the 337-spectrum (7) that in the UV region is the PL spectrum, similar in shape to the UV PL spectrum of toluene, but shifted to longer wavelengths. This part of the spectrum should apparently be attributed to the PL of some impurities in toluene. The main contribution to the PL 337-spectrum in the range 24000–17000 cm^{-1} is associated with

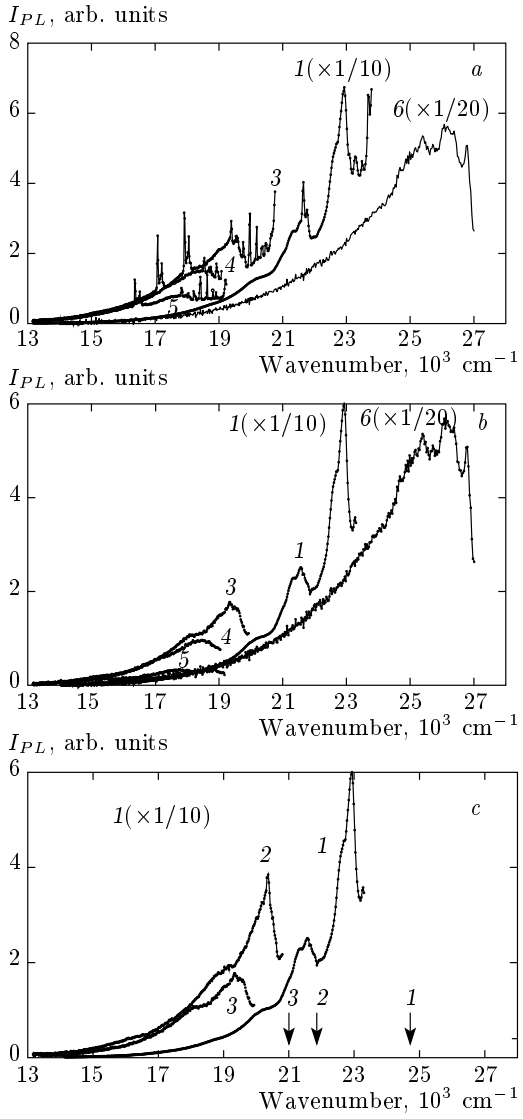

Fig. 8. Photoluminescence spectra of shungite toluene dispersion at 80 K (a) as observed, (b) after the subtraction of Raman scattering of toluene, and (c) attributed to individual GQDs only. Numbers from *1* to *5* denote the same λ_{exc} as in Fig. 4 and number *6* marks $\lambda_{exc} = 337.1$ nm

the emission of all GQDs available in the dispersion. This spectrum is broad and structureless, which apparently indicates the structural inhomogeneity of GQD colloids.

The PL 405- and 476-spectra (*1* and *3*) in the range 23000–17000 cm^{-1} should be attributed to the second group. Both spectra have a clearly defined structure that is most distinctly expressed in the 405-spectrum. The spectrum is characteristic of a complex molecule with allowed electron transitions. Assuming that the maximum frequency at 22910 cm^{-1} determines the position of a pure electron transition, the longer wavelength doublet at 21560–21330 cm^{-1} can be interpreted as vibronic transitions. The distance between the doublet peaks and the pure electron band is 1350–1580 cm^{-1}, which is consistent with the frequencies of totally symmetric vibrations of the C–C graphene skeleton, commonly observed in Raman spectra. Similarly, two peaks of the much less intensive 476-spectrum, which are wider than in the previous case, are divided by the average frequency of 1490 cm^{-1}. The PL 457-spectrum shown in Fig. 8*c* (curve *2*) is similar to spectra *1* and *3*, closer to the 405-spectrum in intensity. All the three spectra are related to individual rGO fragments, albeit of different size that gradually increases in going from the 405-spectrum to 457- and 476-spectra.

The shape of 496- and 514-spectra substantially differs from that of the second-group spectra. Instead of the two peaks observed there, a broad band is observed in both cases. This feature makes these spectra attributable to the third group, to be associated with the appearance of not individual frozen GQDs but their possible clusters (such as dimeric homo- (GQD+GQD) and hetero- (GQD+toluene) structured charge transfer complexes, and so forth). The evidence for such a possibility is discussed in the next section.

The conducted spectral studies of the rGO-Sh toluene dispersions once again confirmed the status of toluene as a good solvent and a good crystalline matrix, which allows obtaining structured spectra of individual complex molecules under conditions when in other solvents the molecules form fractals. This ability of toluene for the first time allowed obtaining the spectra of both individual GQDs and their small clusters. This finding represents the first reliable empirical basis for further theoretical treatment of the spectra observed.

6. DISCUSSION

As follows from the results presented in the previous sections, rGO-Sh dispersions are colloidal dispersions regardless of the solvent (be it water, carbon tetrachloride, or toluene). The dispersion colloid structure depends on the solvent and is therefore substantially different. This issue deserves a special investigation. Thus, the replacement of water with carbon tetrachloride leads to multiple enlargement of pristine colloids, which promotes the formation of a quasi-crystalline image of the condensate structure. At present, the colloid

detailed structure remains unclear. In contrast to carbon tetrachloride, toluene causes the decomposition of pristine colloids into individual rGO fragments. The last facts cast doubt on the possible direct link between the structure of dispersion fractals and the elements of the fractal structure of solid shungite or its post-treated condensate. The observed solvent-stimulated structural transformation is a consequence of the geometric peculiarities of the behavior of fractals in liquids [24]. The resulting spectral data can be the basis for further study of this effect.

The spectral behavior of the aqueous and CTC-dispersions with large colloids is quite similar, although the latter significantly differ in size and structure. Moreover, the features of the PL spectra of these dispersions practically replicate patterns that are typical for the aqueous rGO-Sy dispersions discussed in detail in Sec. 1. This allows us to conclude that the same structural element of the colloidal aggregates of both rGO-Sh dispersions and rGO-Sy one is responsible for the emission, in spite of a pronounced morphological difference in its packing in all these cases. According to the modern view on the shungite structure [22] and a common opinion on the origin of synthetic GQDs [11, 12], rGO fragments about 1 nm in size should play a role, representing GQDs of the rGO colloidal dispersions in all the cases.

Specific effects of toluene, which caused the decomposition of pristine particles into individual rGO fragments with their successive embedding into a crystalline matrix of toluene, for the first time allowed obtaining the PL spectrum of individual rGO fragments. Obviously, the resulting fragments are of different size and shape, which determines the structural inhomogeneity of toluene dispersions. This feature of toluene dispersions is common with other dispersions and explains the dependence of PL spectra on λ_{exc}, which is the main spectral feature of GQDs, both synthetic [11, 12] and of shungite origin.

The structural inhomogeneity of GQDs colloidal dispersions is mainly caused by two reasons, internal and external. The internal reason concerns the uncertainty in the structure (size and shape) of the basic rGO fragments. It is the most significant for shungite while, under laboratory conditions, the rGO fragments structure might be more standardized [11, 12]. Nanosize rGO basic structural elements of solid shungite are formed under the conditions of intense competition of different processes [22], among which the most significant are: (1) natural graphenization of carbon sediments, accompanied by simultaneous oxidation of the graphene fragments and their reduction in water vapor; (2) the retention of water molecules in space between fragments and escape of the water molecules from the space into the environment, and (3) the multilevel aggregation of rGO fragments providing the formation of a monolithic fractal structure. Naturally, the achieved balance between the kinetically-different-factor processes is significantly influenced by random effects, such that the rGO fragments of natural shungite that survived during natural selection are statistically averaged over a wide range of fragments that differ in size, shape, and chemical composition.

Obviously, the reverse procedure of shungite dispersing in water is statistically also nonuniform with respect to colloidal aggregates, and therefore there is a strong dependence of the dispersions on the technological protocol, which results in a change in the dispersion composition caused by slight protocol violations. This (in a sense, a kinetic instability of dispersing) is the reason that the composition of colloidal aggregates can vary when water is displaced by another solvent. The conducted spectral studies have confirmed these assumptions.

An external reason is the fractal structure of colloidal aggregates. The fractals themselves are highly inhomogeneous and, moreover, strongly depend on the solvent. The two reasons determine the feature of the GQD spectra in aqueous and CTC-dispersions, while the first one dominates in the case of toluene dispersions. In view of this, photonics of GQDs has two faces, one of which is of the rGO nature and the other concerns fractal packing of GQDs. As follows from the foregoing, the spectrum study is quite efficient in exhibiting this duality.

The structural PL spectra allow asking the question of identifying the interaction effect of dissolved rGO fragments with each other and with the solvent. Nanosize rGO fragments have high donor-and-acceptor abilities (low ionization potential and high electron affinity) and can exhibit both donor and acceptor properties, with fragment clusters (dimers, trimers, and so forth) being typical charge transfer complexes. Besides this, toluene is a good electron donor, and it can therefore form a charge-transfer complex with any rGO fragment that acts as an electron acceptor. The spectrum of electron–hole states of the complex, which depends on the distance between the molecules and on the initial parameters, is similar to the electron–hole spectrum of clusters of fullerenes C_{60} themselves and of those with toluene [20], positioned by the energy in the region 20000–17000 cm^{-1}. By analogy with nanophotonics of fullerene C_{60} solutions [20], the enhancement of the Raman spectrum of toluene is due to a superposi-

tion of the spectrum over the spectrum of electron–hole states, which follows from the theory of light amplification caused by nonlinear optical phenomena [31]. Additionally, the formation of rGO-toluene charge transfer complexes may promote the formation of stable chemical composites in the course of photochemical reactions [32], which might be responsible for the PL third-group spectra observed in toluene dispersions. Certainly, this assumption requires further theoretical and experimental investigation.

7. CONCLUSION

Photonics of shungite colloidal dispersions faces the problem that great statistical inhomogeneity inherent in the quantum dot as an object of study makes it difficult to interpret the results in detail. Consequently, most important become common patterns that are observed on the background of this inhomogeneity. In the case of the considered dispersions, the common patterns include, primarily, the dispersion PL in the visible region, which is characteristic of large molecules consisting of fused benzenoid rings. This allowed confirming the earlier findings that graphene-like structures of limited size, namely, rGO fragments are the basic structural elements for all the dispersions. The second feature concerns the dependence of the position and intensity of selective PL spectra on the exciting light wavelength λ_{exc}. This feature lies in the fact that regardless of the dispersion composition, and solvent the PL excitation at 405 and 457 nm provides the highest PL intensity, while excitation at either longer or shorter wavelengths produces a much lower emission intensity. The answer to this question must be sought in the calculated absorption and photoluminescence spectra of graphene quantum dots, which we attribute to nanoscale fragments of reduced graphene oxide.

The financial support provided by the Ministry of Science and High Education of the Russian Federation (grant No. 2.8223.2013), Basic Research Program (RAS) Earth Sciences, Section 5, and the RFBR (grant No. 13-03-00422) is greatfully acknowledged. The authors are grateful to A. E. Goryunov for assisting in preparing the dispersions.

REFERENCES

1. B. Trauzettel, D. V. Bulaev, D. Loss, and G. Burkard, Nature Phys. **3**, 192 (2007).
2. A. Güçlü, P. Potasz, and P. Hawrylak, Phys. Rev. B **84**, 035425 (2011).
3. K. A. Ritter and J. W. Lyding, Nature Mater. **8**, 235 (2009).
4. D. Pan, J. Zhang, Z. Li, and M. Wu. Adv. Mater. 22, 734 (2010).
5. J. Shen, Y. Zhu, C. Chen, and C. Li, Chem. Comm. **47**, 2580 (2011).
6. Z. Z. Zhang and K. Chang, Phys. Rev. B **77**, 235411 (2008).
7. V. Gupta, N. Chaudhary, R. Srivastava et al., J. Amer. Chem. Soc. **133**, 9960 (2011).
8. R. Liu, D. Wu, X. Feng, and K. Müllen, J. Amer. Chem. Soc. **133**, 15221 (2011).
9. Y. Li, Y. Hu, Y. Zhao et al., Adv. Mater. **23**, 776 (2011).
10. X. T. Zheng, A. Than, A. Ananthanaraya et al., ACS Nano **7**, 6278 (2013).
11. L. Tang, R. Ji, X. Cao et al., ACS Nano **6**, 5102 (2012).
12. L. Li, G. Wu, G. Yang et al., Nanoscale **5**, 4015 (2013).
13. X. Zhou, Y. Zhang, C. Wang et al., ACS Nano **6**, 6592 (2012).
14. Y. Dong, C. Chen, X. Zheng et al., J. Mater. Chem. **22**, 8764 (2012).
15. M. Zhang, L. Bai, W. Shang et al., J. Mater. Chem. **22**, 7461 (2012).
16. L. Lin and S. Zhang, Chem. Comm. **48**, 10177 (2012).
17. S. Chen, J.-W. Liu, M. L. Chen et al., Chem. Comm. **48**, 7637 (2012).
18. B. S. Razbirin, E. F. Sheka, A. N. Starukhin et al., Pis'ma v ZhETF **87**, 159 (2008).
19. E. F. Sheka, B. S. Razbirin, A. N. Starukhin et al., J. Eksp. Theor. Phys. **135**, 848 (2009).
20. B. S. Razbirin, E. F. Sheka, A. N. Starukhin et al., Fiz. Tverdogo Tela **51**, 1315 (2009).
21. E. F. Sheka, B. S. Razbirin, A. N. Starukhin et al., J. Nanophoton. **3**, 033501 (2009).
22. E. F. Sheka and N. N. Rozhkova, Int. J. Smart Nano Mat. **5** (2014), DOI: 10.1080/19475411.2014.885913.
23. B. S. Razbirin, N. N. Rozhkova, E. F. Sheka et al., in *Advanced Carbon Nanostructures*, Int Conf., St. Petersburg (2013), p. 69.

24. T. A. Witten, in *Soft Matter Physics*, ed. by M. Daoud and C. E. Williams, Springer-Verlag, Berlin–Heidelberg (1999), p. 261.

25. J.-F. Gouyet, *Physics and Fractal Structures*, Springer, Paris–New York (1996).

26. S. Park, J. An, I. Jung et al., Nano Lett. **9**, 1593 (2009).

27. C. E. Hamilton, J. R. Lomeda, Z. Sun et al., Nano Lett. **9**, 3460 (2009).

28. N. N. Rozhkova, G. I. Emel'yanova, L. E. Gorlenko et al., Fiz. Khim. Stekla **37**, 853 (2011).

29. E. V. Shpol'skii, Uspekhi Fiz. Nauk **71**, 215 (1960).

30. N. N. Rozhkova, *Nanouglerod Shungitov* (*Shungite Nanocarbon*), Karelian Research Centre of RAS, Petrozavodsk (2011).

31. J. P. Heritage and A. M. Glass, in *Surface Enhanced Raman Scattering*, ed. by R. K. Chang and T. E. Furtak, Plenum Press, New York–London (1982), p. 391.

32. E. F. Sheka, Nanosci. Nanothechn. Lett. **3**, 28 (2011).